Metal–ligand ring aromaticity in a 2D coordination polymer used as a photosensitive electronic device

Article *in* New Journal of Chemistry · January 2019

DOI: 10.1039/C8NJ05526B

CITATIONS
19

READS
289

8 authors, including:

Faruk Ahmed
Dhaka International University
54 PUBLICATIONS **6,657** CITATIONS
SEE PROFILE

Sourav Ranjan Ghosh
Heritage Institute of Technology
10 PUBLICATIONS **40** CITATIONS
SEE PROFILE

Soumi Halder
Jadavpur University
19 PUBLICATIONS **359** CITATIONS
SEE PROFILE

Surajit Guin
Behala College
9 PUBLICATIONS **23** CITATIONS
SEE PROFILE

NJC

PAPER

View Article Online
View Journal

Cite this: DOI: 10.1039/c8nj05526b

Metal–ligand ring aromaticity in a 2D coordination polymer used as a photosensitive electronic device†

Faruk Ahmed,[a] Sourav Ranjan Ghosh,[bc] Soumi Halder,[d] Surajit Guin,[b] Seikh Mafiz Alam,[a] Partha Pratim Ray, *[d] Atish Dipankar Jana *[b] and Mohammad Hedayetullah Mir *[a]

Received 31st October 2018,
Accepted 8th January 2019

DOI: 10.1039/c8nj05526b

rsc.li/njc

In this study, aromaticity of a 14-membered metal–ligand ring present in a two-dimensional coordination polymer (2D CP), $[Zn_2(fum)_2(4\text{-phpy})_4(H_2O)_2]$ (**1**) (H_2fum = fumaric acid and 4-phpy = 4-phenyl pyridine), was theoretically investigated by calculating the nucleus-independent chemical shifts (NICS). Furthermore, the calculation was supported by free of in-plane component NICS (FiPC-NICS) used specifically for inorganic heterocycle and electron localization function (ELF) analysis. The calculations reveal that the metal–ligand ring has an aromatic character and a moderate C–H···π interaction energy (−8.56 kcal mol^{-1} at the HF/6-311++G(d,p) level of theory) of 4-phpy with the 14-membered ring, which plays an active role in the molecular self-assembly for crystal packing. Furthermore, the compound **1** has a substantive photosensitivity with an appreciable on–off ratio; therefore, this material can be used as a photosensitive electronic device.

Introduction

In chemistry, noncovalent or supramolecular interactions involving π-systems are of significant importance.[1,2] These interactions are accountable for the stabilization of many important molecular systems including large biological systems *e.g.* nucleic acids and proteins.[3–6] Moreover, these weak forces control the orientations of molecular species in crystalline lattices. Hence, they are considered as one of the key factors in crystal engineering.[7] The role of classical hydrogen bonding in supramolecular assemblies has been widely investigated for many years,[8,9] and this type of bonding is considered as a structural motif in crystal engineering. Moreover, π···π stacking,[2] C–H···π interactions,[10] van der Waals interactions[11,12] and halogen···halogen interactions[13,14] have been studied over the past few years through theoretical studies with a view of their utilization in the deliberate design of supramolecular aggregates in crystal engineering. In addition, various groups have reported the existence of a new type of supramolecular interactions by both experimental and theoretical studies. Anion···π,[15] cation···π,[16] π(chelate)···π(chelate) stacking[17,18] and C–H···π(chelate)[19–23] are some examples of these interactions, which have been extensively studied in the context of crystal packing. Among these, the C–H···π(chelate) interactions have attracted particular attraction since a metal–chelate ring has the possibility to reveal aromatic character within the chelate ring.

Although the concept of aromaticity was initiated to describe π-electron delocalized, cyclic and planar organic molecules having $(4n + 2)\pi$ electrons,[24] the perception was extrapolated to metal–chelate ring clusters and organometallic compounds. Moreover, a number of metal–chelate rings have been structurally and theoretically characterized in the context of aromaticity, called metalloaromaticity.[25–28] However, large membered metal–ligand rings showing an aromatic character have rarely been reported in the literature.

Moreover, metal–organic coordination polymers (CPs), also known as metal–organic frameworks (MOFs), are an emerging class of materials constructed from metal ion centres or metal clusters and organic linkers.[29–35] The design and synthesis of CPs is an area of crystal engineering that is widely investigated to realize how crystalline materials can be engineered.[36–41] In the CPs described to date, the employment of supramolecular interactions for the construction of high-dimensional networks

[a] Department of Chemistry, Aliah University, New Town, Kolkata 700 156, India. E-mail: chmmir@gmail.com
[b] Department of Physics, Behala College, Parnasree, Kolkata, 700 060, India. E-mail: atishdipankarjana@yahoo.in
[c] Department of Physics, Heritage Institute of Technology, Kolkata 700 107, India
[d] Department of Physics, Jadavpur University, Jadavpur, Kolkata 700 032, India. E-mail: partha@phys.jdvu.ac.in

† Electronic supplementary information (ESI) available: Fig. S1–S5, TGA, PXRD, FESEM, Hirshfeld surface analysis, ELF study, Tables S1 and S2, H-bonding, C–H···π and π···π interactions, theoretical data and X-ray crystallographic data in CIF format for compound **1**. CCDC 1550370 (**1**). For ESI and crystallographic data in CIF or other electronic format see DOI: 10.1039/c8nj05526b

has been less explored. As a continuation of our study to reveal the role of supramolecular interactions in the construction of higher dimensional CPs and to establish their physical properties,[42–44] herein, a new fumarate-based 2D CP $[Zn_2(fum)_2(4\text{-phpy})_4(H_2O)_2]$ (**1**) (H_2fum = fumaric acid and 4-phpy = 4-phenyl pyridine) was synthesized using pyridyl as a co-ligand, which formed a 3D supramolecular aggregate *via* the combination of π···π and C–H···π interactions. Interestingly, the compound **1** contains a 14-membered metal–ligand ring with two Zn(II) centres bridged by two fumerate dianions, which makes the structure quite fascinating. Analysis of the crystal structure reveals that this metal–ligand ring can be a hydrogen acceptor in the C–H···π interactions. Computations show that this metal–ligand ring has an aromatic character. To the best of our knowledge, this is the first example of a 14-membered metal–ligand ring showing an aromatic character. Moreover, the compound **1** exhibits photosensitivity with an appreciable on–off ratio. Current conductivity under dark and illumination shows a non-linear rectifying behaviour. Herein, π···π interactions seem to play a significant role in charge transport through space mechanism.

Experimental

Materials and physical method

All chemicals purchased were of reagent grade and used without further purification. Elemental analysis (carbon, hydrogen and nitrogen) was performed using the Perkin–Elmer 240C elemental analyzer. Infrared spectrum in KBr (4500–500 cm^{-1}) was obtained using the Perkin–Elmer FTIR spectrum RX1 spectrometer. Thermogravimetric analysis was conducted using the Perkin–Elmer Pyris Diamond TG/DTA in the temperature range between 30 °C and 600 °C under a nitrogen atmosphere at the heating rate of 12 °C min^{-1}. PXRD data was obtained *via* the Bruker D8 Advance X-ray diffractometer using CuK_α radiation (λ = 1.548 Å) generated at 40 kV and 40 mA. The PXRD spectra were obtained in the 2θ range of 5°–50°. Structural characterisation of the synthesized material was carried out by the FEI make Inspect F50 field emission scanning electron microscope (FESEM). Electrical characterization was performed using the Keithley 2400 source meter, interfaced with PC.

Synthesis of compound 1

Synthesis of compound **1**: a solution of 4-phpy (0.031 g, 0.2 mmol) in MeOH (2 mL) was slowly and carefully layered to a solution of $Zn(NO_3)_2{\cdot}6H_2O$ (0.059 g, 0.2 mmol) in H_2O (2 mL) using a 2 mL 1 : 1 (= v/v) buffer solution of MeOH and H_2O followed by layering of H_2fum (0.023 g, 0.2 mmol) neutralized with Et_3N (0.021 g, 0.2 mmol) in 2 mL EtOH. Block-shaped colourless crystals of $[Zn_2(fum)_2(4\text{-phpy})_4(H_2O)_2]$ **1** were obtained after three days (0.071 g; yield 70%). Elemental analysis (%) calcd for $C_{52}H_{44}N_4O_{10}Zn_2$: C 61.44, H 4.33, N 5.51; found: C 61.94, H 4.67, N 5.64. IR (KBr pellet, cm^{-1}): 1542 $\nu_{as}(COO^-)$, 1362 $\nu_{sys}(COO^-)$.

General X-ray crystallography

Single crystals of compound **1** having suitable dimensions were used for data collection using the Bruker SMART APEX II diffractometer equipped with graphite-monochromated MoK_α radiation (λ = 0.71073 Å). The molecular structure was solved using the SHELXL-97 package.[45] Non-hydrogen atoms were refined using anisotropic thermal parameters. Hydrogen atoms were placed at their geometrically idealized positions and constrained to ride on their parent atoms. Crystallographic data for **1** is summarized in Table S1 (ESI†), and selected bond lengths and bond angles are listed in Table S2 (ESI†).

Device fabrication and characterization

At first, for device fabrication, a fluorine-doped tin oxide (FTO)-coated glass substrate was cleaned by ultrasonication in an isopropanol medium for 15 min. Then, the glass substrate was cleaned in acetone and distilled water successively. After being washed properly, the FTO-coated glass substrate was dried in a vacuum chamber. Moreover, a visually homogeneous dispersed solution of the sample was prepared in the dimethyl sulfoxide (DMSO) solvent. This dispersed sample was spin-coated onto the FTO-coated glass substrate at the rate of 400 rpm using the SCU 2700 spin coating unit in vacuum. At the last step of device fabrication, aluminum (Al) was deposited onto the spin-coated film using the 12A4D HINDHIVAC vacuum coating unit at a pressure of 10^{-6} Torr. Moreover, the fabricated film thickness was measured as 9 μm using the DEKTAK surface profiler.

Methodology of DFT computation

To explore the electronic structure of the two subcomponents of the fum-bridged Zn(II) units present in the 2D coordination polymer, geometry optimizations were performed using DFT computations. All calculations were performed using the Gaussian 03 package.[46] Initial geometries of the respective subunits were adopted from the crystal structure, and geometry optimizations for each subunit were carried out at the DFT 6-311G level of theory using the B3LYP hybrid density functional. The binding energies of the four weak intermolecular interactions, *i.e.* (i) the C–H···π interaction of 4-phpy with the 14-membered metal-fumarate ring, (ii) the π···π interaction of two 4-phpy molecules, and two C–H···π interactions (iii) one at 2.79 Å and (iv) another at 3.00 Å (see Fig. 2) were estimated in this study. Geometries of the selected models (see Fig. 5 and Fig. S5, ESI†) were adopted from the crystal structure, and binding energies were estimated without optimization to have an idea of the relative importance of these four weak intermolecular forces present in the crystal structure. The basis set superposition error-corrected binding energy (B.E.) of the C–H···π interaction of 4-phpy with the 14-membered metal-fumarate ring has been estimated at the HF level of theory using both the 6-31G(d,p) and the 6-311++G(d,p) basis sets. Note that the basis set dependency was found to be small; the basis set correction was estimated employing counterpoise methodology as implemented in the Gaussian 03 package. The B.E. of each motif was estimated by calculating the difference in the energies of the interacting system of two components together as well as the sum of the energies of the individual components. Both these energies were computed at the same level of theory. Dispersion-corrected DFT computations conducted using the M06-2X density functional and 6-31G(d,p) basis set were employed to estimate the

binding energies of all four weak forces. For this computation, the GAMESS-2016 version 2016-pgi-linux-mkl program package was used.[47]

All SCF-GIAO calculations presented herein were carried out using the SCF-GIAO (SCF with GIAOs) methodology[48,49] as implemented in the Gaussian 03 program package. Both the HF and DFT methodology were employed in the NICS calculations. It has been verified that the NICS values do not change very much with the different level of theory (HF or DFT) employing different basis sets (6-311G, 6-31G(2d), 6-31G(d,p)) and density functional (B3LYP, X3LYP). Electron localization function (ELF) reported in the present study was generated using the Multiwfn-3.6 package[50] for which the input wave function was computed at the DFT B3LYP/6-311++g(d,p) level of theory using the Gaussian 03 package.[46]

Results and discussion

Structural descriptions of $[Zn_2(fum)_2(4\text{-phpy})_4(H_2O)_2]$ (1)

Colourless block crystals of **1** were obtained using diffusion of 4-phpy and H_2fum in ethanol into a solution of aqueous $Zn(NO_3)_2{\cdot}6H_2O$ and Et_3N in H_2O/MeOH. Single-crystal X-ray crystallography reveals that the compound **1** crystallizes in the monoclinic space group $P2_1/n$ with Z = 4. There are two independent Zn(II) centers present in the asymmetric unit, in which both the Zn1 and Zn2 have distorted octahedral geometry, as shown in Fig. 1a. Zn2 is ligated to two O atoms from two fum anions in a monodentate fashion, two O atoms from two aqua ligands in the equatorial plane, and two N atoms from two 4-phpy ligands at the axial position. On the other hand, two N atoms from two 4-phpy ligands and four O atoms from three different fum anions are bonded to Zn1 in an octahedral environment. Moreover, two such Zn1 centres were bridged by two dicarboxylate ligands through O3 and O9 in a manner such that a 14-membered macrocyclic metal–ligand ring, including two Zn1 centres, was formed. The connectivity of the neighbouring carboxylate oxygen atoms with Zn2 centers results in a 2D sheet-like structure with 4-membered and 8-membered rings connected to each other (Fig. 1b). Each 4-membered ring was surrounded by four 8-membered rings, whereas each 8-membered ring was attached with four 4-membered rings. The overall topology was decribed as a 2D 4.8^2-**fes** framework (Fig. S1, ESI†) using the TOPOS program.[51]

In the solid-state structure, the 2D networks were self-assembled *via* strong intermolecular H-bonding between the aqua ligands and the O atoms of the bridging fum ligands with the O···O separation of 2.62–2.85 Å. According to the graph set analysis proposed by Etter,[52] the 2D sheet comprises three different rings (R) with hydrogen bonding interactions: $R_2^2(8)$, $R_2^2(16)$ and $R_4^4(22)$ (Fig. S2, ESI†). However, these 2D H-bonded networks further fabricate 3D supramolecular aggregates *via* face-to-face π···π stacking at a centroid–centroid distance of 3.69 Å and two set of edge-to-face C–H···π interactions; the H···π distance in one set is 2.79 Å, and in another set, it is 3.00 Å (Fig. 2). The dispersion-corrected interaction energy computed at the DFT\M06-2X\6-31G(d,p) level of theory for the π···π interaction between a pair of 4-phpy molecules is −7.44 kcal mol^{-1}. At the same level of theroy, the interaction energy for C–H···π interaction at 2.79 Å is −4.61 kcal mol^{-1} and that of the C–H···π interaction at 3.00 Å is −3.50 kcal mol^{-1} (Fig. S3, ESI†).

A closer observation at the connectivity of Zn1 centres and fum ligands reveals the presence of a 14-membered ring comprising two Zn(II) centres and two fum ligands. The 4-phpy ligand attached to the metal centre located on one layer interacts with the 14-membered metal–ligand ring of the adjacent layer in an edge-to-face C–H···π (metal–ligand ring) interaction with an almost optimal angle for a perfect T-shaped geometry (Fig. S4, ESI†).

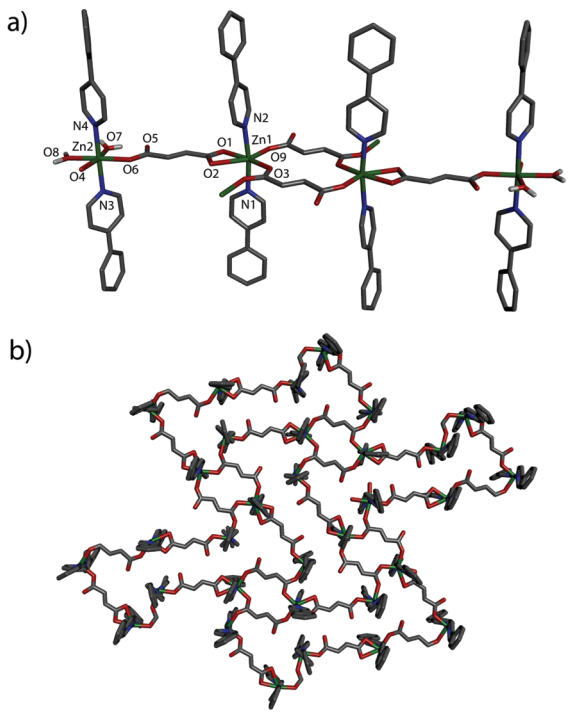

Fig. 1 (a) Basic structural unit showing the coordination environment around the metal centres. (b) A part of 2D structural network showing the 4.8^2-**fes** framework. H-atoms are not shown for clarity.

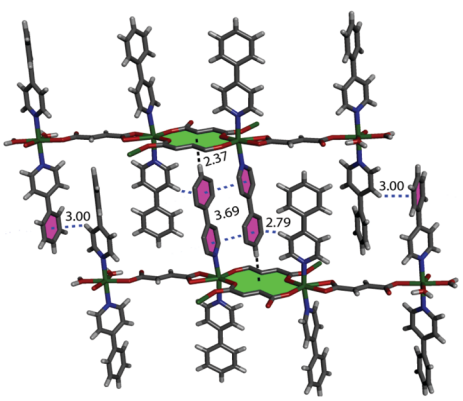

Fig. 2 π···π, C–H···π and C–H···π (14-membered metal–ligand ring) Interactions in **1**. Distances in Å.

Moreover, the distance of the hydrogen atom attached to the phenyl ring of 4-phpy to the centroid of the metal–ligand ring is 2.37 Å.

Analysis of the NICS results

NICS scan over the 14-membered ring plane. To assess the aromatic nature of the relevant ring, nucleus independent chemical shift (NICS)[53] calculations have been performed, which is a well-accepted parameter in the scientific community as an indicator of the aromatic nature of planar chemical systems.[54] Negative NICS values indicate aromaticity, and positive NICS values indicate antiaromaticity. Often, NICS(0) and NICS(1) values have been reported in the literature as a measure of aromaticity.[55,56] However, NICS(0) is calculated at the ring plane ($Z = 0$), and NICS(1) is the value of NICS at 1 Å above the mean plane. Fig. 3 shows the variation of NICS(0) over the ring plane calculated at the HF/6-311G level of theory. Note that the zero iso-contour line separates the small central region of the ring from the negative NICS(0) region. The negative NICS(0) value varies between 0 and 5 over most of the region of the 14 membered circuit constituted by two fum ligands and two Zn(II) ions. On moving along the x-axis (joining fum O atoms as shown in Fig. 4) or the y-axis in the ring plane, the NICS value increases from −5 to −20, closer to the atoms over the ring. Therefore, most of the central region of the ring has a small negative NICS(0) values; however, the negative value increases towards the periphery of the ring. As is well-known, NICS(0) is often corrupted by contribution from orbitals other than π-orbitals; thus, NICS(1) as well as NICS(z) at other heights are often considered to assess the aromatic nature of planar benzene-like chemical systems.[55–57] For more complex systems, particularly rings containing hetero atoms and metal centres, the distribution of NICS values over the surface of the ring at different heights is considered. By carrying out surface scan at various heights, the NICS field in a 3D space can be obtained.

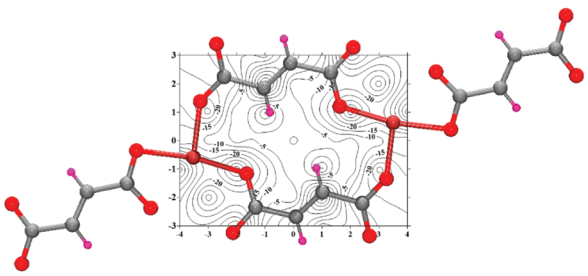

Fig. 3 Variation of NICS(0) over the surface of the 14-membered metal ligand ring.

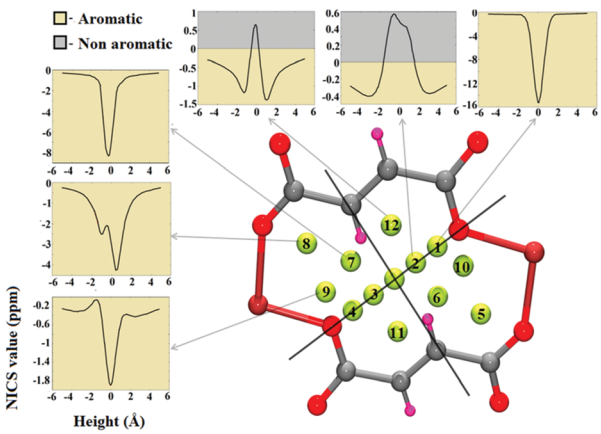

Fig. 4 Variation of NICS with height at twelve different positions in the 14-membered ring plane. Variation of NICS(z) has been shown only for one set of symmetry-related locations.

Variation of NICS with height at different points over the ring plane. NICS(0) at the ring centroid is positive (1.6956 ppm at HF/6-311G level); however, above or below the mean plane of the ring along the z-direction, the NICS value becomes negative around a height 1.75 Å. The NICS value becomes maximum negative at a height of 3 Å, and then, its magnitude slowly decreases, but the sign remains negative (Fig. S5, ESI†). Variation of NICS with height (hereinafter mentioned as NICS(z)) at twelve points other than the ring centroid (0,0,0) has been depicted in Fig. 4. These points were selected in a way such that the points (1, 4); (2, 3); (5, 8); (6, 7); (9, 10) and (11, 12) are centro-symmetrically related to each other with respect to the centroid of the ring. For (1, 4), (5, 8), (6, 7), and (9, 10), NICS(0) and NICS(z) are always negative (Table S6, ESI†). For (2, 3) and (11, 12), NICS(0) is positive; however, as the height increases beyond 1.5 Å for (2, 3) and 0.5 Å for (11, 12), the NICS value becomes negative. We studied the variation of NICS with height from −5 Å to 5 Å on either side of the ring plane. Each symmetry-related pair of points shows almost the same variation of the NICS(z) value. Maximum negative NICS value (−16 ppm) was observed for the points (1) and (4). Although the computed NICS values are method-dependent, the general trend of variation of NICS(z) is same for the HF and DFT method with various basis sets and density functional (Table S7, ESI†). This variation of NICS(z) for point (1) has been depicted in Fig. S5, ESI.† Benzene is a prototypical organic aromatic system whose NICS value is around −8.0 ppm.[58] For the current metal–ligand macrocycle, the NICS(0) symmetrically varies over the ring plane, and the negative NICS value increases towards the periphery. The highest negative NICS value −16 ppm at the point 1 and 4 is more than that of benzene. Since benzene is a purely organic system, its comparison with inorganic aromatic systems is more important. Recently, many chelate ring systems have been explored for possible aromaticity.[25,59] NICS calculations for acetylacetonato (acac) and *o*-benzoquinonediimine (bqdi) have demonstrated that although most chelates of these ligands do not show higher negative NICS values, the Ru^{2+}-bqdi chelate ring has higher negative NICS(0) values (−8.52 ppm).[25] However, NICS studies of Ni-containing chelate rings of 1,2-diaminoethane (NICS(0) = −30.19 ppm), 1,3-diaminopropane (NICS(0) = −16.10 ppm) and 1,4-diaminobutane (NICS(0) = −10.06 ppm) show quite appreciable negative NICS(0) values.[59] NICS calculation of the dicupra[10]-annulene system shows that the $NICS(0)_{zz}$ value can be as high as −34.8 ppm. A comparison of the NICS values of the present 14-membered metal–ligand ring with the abovementioned systems shows that this ring falls in the same group of metal–ligand aromatic systems.

FiPC-NICS study of the 14-membered ring. Although NICS is one of the most widely used aromaticity index, there is no universally accepted indicator of aromaticity. Therefore, indiscriminate use of NICS as an aromaticity indicator has been cautioned.[55,60,61] In particular, for inorganic heterocycles, a new modified NICS index called free of in-plane component NICS (FiPC-NICS) has been recently introduced.[61] FiPC-NICS has evolved from the idea that NICS can be decomposed into three components: NICS = $-1/3(\sigma_{xx} + \sigma_{yy} + \sigma_{zz})$, which can be reorganized as NICS = ($NICS_{in\text{-}plane}$ + $NICS_{out\text{-}plane}$), where $NICS_{in\text{-}plane} = -1/3(\sigma_{xx} + \sigma_{yy})$ and $NICS_{out\text{-}plane} = -1/3(\sigma_{zz})$.[55] To estimate FiPC-NICS, the NICS profile is computed along the axis perpendicular to the molecular plane and then decomposes into in-plane and out-plane components. When a graph of in-plane *vs.* out of plane components of NICS is plotted, three cases may arise: (i) linear, (ii) concave, or (iii) convex. Concave nature of the graph indicates antiaromaticity, and convex nature indicates aromaticity. On the other hand, linear variation indicates a non-aromatic character. We have computed FiPC-NICS for the 14-membered ring at point (1). The graph of $NICS_{in\text{-}plane}$ *vs.* $NICS_{out\text{-}plane}$ has been depicted in Fig. 5, and the data is presented in Table S8, ESI.† The graph shows a convex variation, which means the present fum-bridged metal–ligand ring has an aromatic character. Moreover, FiPC-NICS for benzene shows a similar nature;[61] recently, FiPC NICS has been applied to other systems.[62–64]

From NICS as well as FiPC-NICS studies, it can be concluded that the 14-membered ring possesses an aromatic character. This metal–ligand ring is involved in the C–H···π interaction of the phenyl part of the axially bound 4-phpy ligand. The 4-phpy molecule attached to the metal center of one layer interacts with the 14-membered metal–ligand ring situated on an adjacent layer in an edge to face C–H···π (metal–ligand ring) interaction. As shown in Fig. 6 (Table S9, ESI†), the interaction energy has been computed to be −8.56 kcal mol^{-1} (HF/6-311++G(d,p) level). At the DFT/M06-2X/6-31G(d,p) level, this interaction energy is −13.62 kcal mol^{-1} (Table S10, ESI†). The M06-2X density functional is capable of considering the dispersion correction.

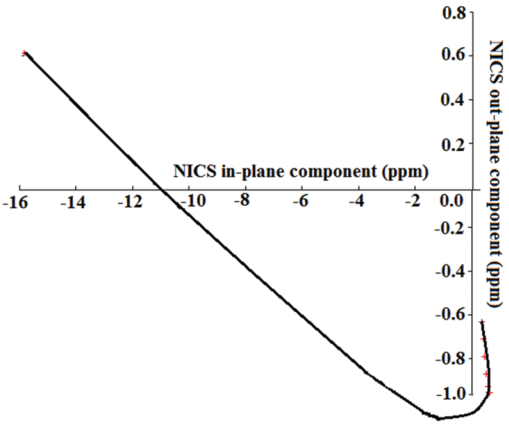

Fig. 5 The plot of NICS in-plane *vs.* NICS out-plane at the point (1) of the 14-membered ring.

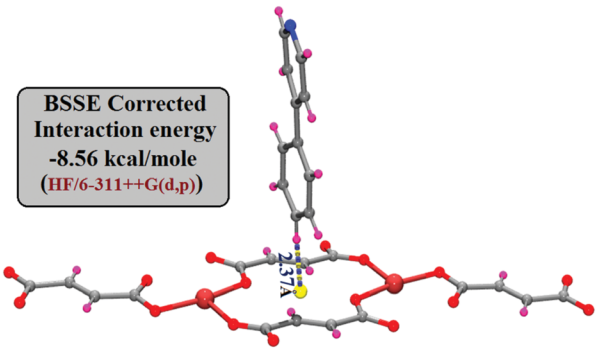

Fig. 6 CH···π interaction of the 4-phpy molecule of one layer with the 14-membered metal–ligand ring.

Therefore, much higher interaction energy at the DFT/M06-2X/6-31G(d,p) level indicates that dispersion has a strong effect on the intermolecular interaction in the present system. The geometry of the CH···π interaction observed in the crystal structure shows that the H-atom attached to the phenyl ring of 4-phpy is positioned over the center of the 14-membered metal–ligand ring in a region where the computed NICS data have substantial negative values. The computed interaction energy corresponding to the CH···π interaction of 4-phpy with the 14-membered metal–ligand ring is highest as compared to that of the three other weak forces, *i.e.*, π···π interaction between 4-phpy molecules and two CH···π interactions with two different H···π distances (Fig. 2), all of which are involved in the interlayer packing of the CP. The respective interaction energies are −13.6 kcal mol^{-1} (for the metal–ligand ring 4-phpy CH···π interaction), −7.44 kcal mol^{-1} (for 4-phy π···π interaction), −4.61 kcal mol^{-1} (for C–H···π having H···π distance 2.79 Å) and −3.50 kcal mol^{-1} (for C–H···π having H···π distance 3.00 Å) (Table S10, ESI†). Therefore, undoubtedly, the C–H···π interaction associated with the 14-membered metal–ligand ring is the dominant weak force in crystal packing. With this high value of interaction energy, the aromatic nature of the 14-membered metal–ligand ring correlates well.

Electron localization function (ELF) study

Electron localization function (ELF) is another way to study the presence or absence of aromaticity in a system. ELF was first introduced by Becke *et al.*;[65] currently, it is a well recognized index of aromaticity. To characterize the aromaticity of the 14-membered metal–ligand ring, we have studied the ELF apart from the NICS calculations. Bifurcation analysis of the ELF function provides information about the possibility of possessing aromaticity in a system. Generally, a contiguous ELF iso surface with the minimum iso value of 0.70 is an accepted criterion of the presence of aromaticity in a system. Note that ELF is defined in a way such that the ELF iso value for any system ranges between 0.00 and 1.00. The higher the iso value at which bifurcation occurs, breaking the contiguity of the iso-surface over the whole system, the higher the aromaticity of the system.[66] For benzene, the bifurcation threshold is 0.91.[67] The result of the ELF study for the 14-membered ring is shown in Fig. 7, which is the total ELF for the system plotted at four different iso levels. It can be seen

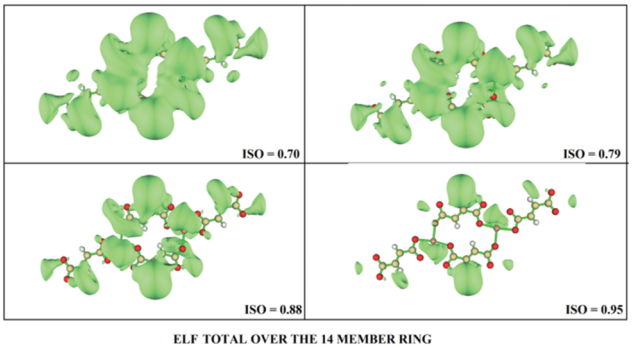

Fig. 7 The total ELF for the 14-membered ring at different iso values.

that at an iso value of 0.70, the ELF function is spread over the 14-membered ring in a contiguous fashion. This contiguity remains intact till an iso value of 0.87, and bifurcation in the ELF iso surface first appears at an iso value of 0.88. This bifurcation level is quiet high and is comparable to the ELF bifurcation value of other standard aromatic systems.[68,69] To have a deeper insight into the nature of the ELF function, it is generally decomposed into ELF_π and ELF_σ.[68,69] While ELF_π provides the information regarding the contribution of the π-orbitals in the aromatic nature of a system, ELF_σ provides information regarding the contribution of the σ-orbitals to aromaticity. ELF_σ and ELF_π for the 14-membered system are shown in Fig. S6, ESI.† Comparison of ELF_π and ELF_σ depicted in Fig. S6 (ESI†) clearly shows that the aromatic nature of the 14-membered ring is mainly due to the contribution of the σ-orbitals. While ELF_π is not continuous over the 14-membered ring at an iso value of 0.71, ELF_σ is continuous. The bifurcation isovlaue of ELF_σ is 0.83, which is slightly less than the bifurcation iso value (0.88) of the total ELF. Therefore, it can be concluded that the aromatic nature of the 14-membered ring is mainly due to the contribution from the σ-orbitals.

TGA, PXRD and FESEM analysis

To verify the thermal stability of the compound **1**, thermogravimetric analysis (TGA) was performed with the fresh sample within the temperature range 30–600 °C under a N_2 atmosphere. The result of the TGA experiment indicates that **1** is stable upto 100 °C (Fig. S7, ESI†). Powder X-ray diffraction (PXRD) has been carried out at room temperature. All major peaks of the PXRD pattern of the as-synthesized **1** matched quite well with those simulated from single crystal data; this indicated phase purity of the bulk (Fig. S8, ESI†). The FESEM study reveals that the synthesized material shows a flake-like structure (Fig. S9, ESI†), which may have influenced the properties of the CP.

Optical analysis

To observe the light absorption property of **1**, the absorption spectrum is obtained (Fig. 8). The spectrum shows that absorption occurs in the visible region with an absorption band edge of ~810 nm. The optical band gap energy (E_g) of the compound was evaluated using the Tauc equation:[70]

$$\alpha h\nu = A(h\nu - E_g)^n \quad (1)$$

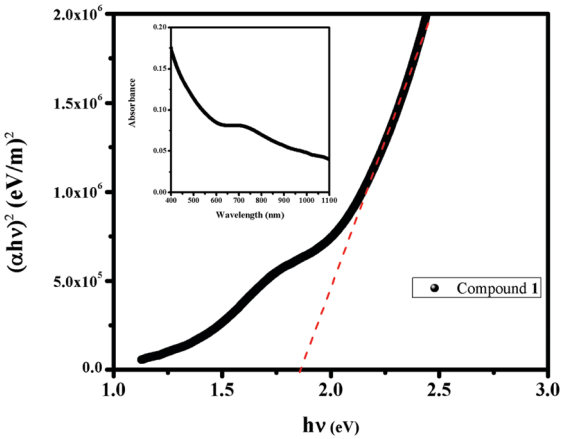

Fig. 8 Tauc plot and UV absorption spectra (inset) of **1**.

where α is the absorption coefficient, E_g is the band gap, h is Planck's constant, ν is the frequency of light, n is the electron transition process constant and c is the constant. To calculate the optical band gap, the value of n is taken as 1/2. The Tauc plot of **1** is shown in Fig. 8. The optical energy band gap (E_g) can be determined by extrapolating the linear region of the plot of $(\alpha h\nu)^2$ *versus* $h\nu$ to $\alpha = 0$, and the value is estimated to be about 1.52 eV.

DFT computation and band gap

As the compound **1** has two types of Zn(II) centres, DFT-optimized geometries and HOMO–LUMO gaps for these two units have been computed. The optimized geometries of both units are of similar nature to that found in the crystal structure. However, the HOMO–LUMO gap of subunit II (Zn1 centre) is 1.867 eV [DFT/b3lyp/6-311++G(d,p)] (Fig. 9), which is in good agreement with the band gap obtained from the Tauc plot. A small deviation in the band gap may be due to geometric factors, which have not been considered while calculating a single motif. Therefore, it may be concluded that the charge transport in **1** occurs through the Zn1 centre through the π-electron cloud.

Electrical analysis

Light absorption of the material has been carried out in the visible region, which indicates that the material has some light-induced properties. Moreover, the optical band gap indicated

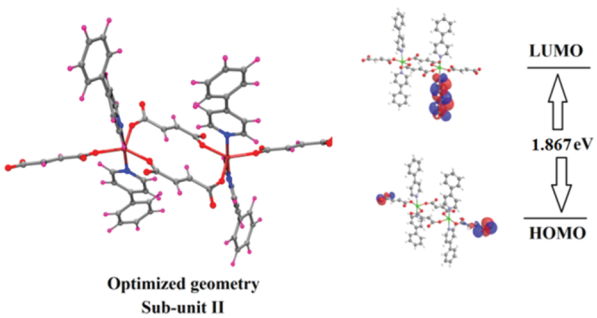

Fig. 9 DFT optimized geometry of the subunit II (Zn1 centre) of **1**.

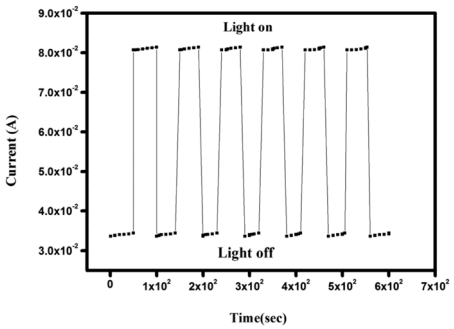

Fig. 10 Plot of photocurrent *vs.* time of compound **1**.

the semiconducting nature of the material; this prompted us to further investigate the electrical properties of the material. The transient photocurrent *vs.* time measurements were performed to study the conducting mechanism of compound **1** (Fig. 10). Herein, we can observe that the photocurrent reaches a certain value on switching on the illumination and then returns to its initial value on switching off. The increase in photocurrent is because of the movement of photoelectrons from HOMO to LUMO. The measurement was obtained for several on/off cycles, and the obtained photosensitivity was 2.42. There was an enhancement of electrical conductivity from 5.14×10^{-3} Sm^{-1} to 5.93×10^{-3} Sm^{-1} under illumination. Herein, the enhancement of conductivity in the presence of light may be because of conformational changes of 4-phpy rings. Inter-layer 4-phpy rings may attain maximum planarity during irradiation.[71]

Conclusions

In summary, we have encountered an interesting 14-membered metal–ligand ring that possesses an appreciable aromatic character. To date, there are only a few reports on aromaticity involving rings formed by transition metals bridged by organic ligands, giving rise to metal–organic complexes.[28,72–74] To the best of our knowledge, this is the first example of a CP containing a 14-membered $Zn_2(fum)_2$ metal–ligand ring showing aromaticity. This study opens up the possibility of a new area of aromaticity involving metallocycles formed through bridging of transition metal centers by organic ligands inside the CPs. With suitable choice of ligands of different lengths and conjugation, it may be possible to engineer metal–ligand rings of different diameters having an aromatic character. In addition, the compound **1** exhibits significant photosensitivity with an appreciable on–off ratio. The electrical transport properties suggest that the synthesized material can be applied in a photosensing device.

Conflicts of interest

There are no conflicts to declare.

Acknowledgements

This work was supported by SERB, India (Grant No. SB/FT/CS-185/2012, dated 30/07/2014) and F. A. thanks the UGC for MANF fellowship. A. D. J. acknowledges the financial support received from the Department of Science, Technology and Biotechnology, Government of West Bengal, India, through the project memo no 250(Sanc.)/ST/P/S&T/16G-47/2017, dated 25/03/2018.

References

1 C. A. Hunter and J. K. M. Sanders, *J. Am. Chem. Soc.*, 1990, **112**, 5525–5534.
2 C. Janiak, *J. Chem. Soc., Dalton Trans.*, 2000, 3885–3896.
3 C. A. Hunter, J. Singh and J. M. Thornton, *J. Mol. Biol.*, 1991, **218**, 837–846.
4 L. Serrano, M. Bycroft and A. R. Fersht, *J. Mol. Biol.*, 1991, **218**, 465–475.
5 S. K. Burley and G. A. Petsko, *Science*, 1985, **229**, 23–28.
6 K. M. Guckian, B. A. Schweitzer, R. X.-F. Ren, C. J. Sheils, D. C. Tahmassebi and E. T. Kool, *J. Am. Chem. Soc.*, 2000, **122**, 2213–2222.
7 G. R. Desiraju and A. Gavezzotti, *J. Chem. Soc., Chem. Commun.*, 1989, 621–623.
8 G. R. Desiraju, *Crystal Engineering, The Design Of Organic Solids*, Elsevier Science, Amsterdam, 1989.
9 C. B. Aakeröy and A. M. Beatty, *Aust. J. Chem.*, 2001, **54**, 409–421.
10 M. Nishio, M. Hirota and Y. Umezawa, *The C–H/π Interaction: Evidence, Nature and Consequences*, Wiley-VCH, New York, 1998.
11 A. J. Fletcher, K. M. Thomas and M. J. Rosseinsky, *J. Solid State Chem.*, 2005, **178**, 2491–2510.
12 A. Schneemann, V. Bon, I. Schwedler, I. Senkovska, S. Kaskel and R. A. Fischer, *Chem. Soc. Rev.*, 2014, **43**, 6062–6096.
13 G. R. Desiraju and R. Parthasarathy, *J. Am. Chem. Soc.*, 1989, **111**, 8725–8726.
14 F. F. Awwadi, R. D. Willett, K. A. Peterson and B. Twamley, *Chem. – Eur. J.*, 2006, **12**, 8952–8960.
15 A. G. Raso, F. M. Alberti, J. J. Fiol, A. Tasada, M. B. Oliver, E. Molins, D. Escudero, A. Frontera, D. Quinonero and P. M. Deya, *Inorg. Chem.*, 2007, **46**, 10724–10735.
16 D. A. Dougherty, *Acc. Chem. Res.*, 2013, **46**, 885–893.
17 D. N. Sredojević, Z. D. Tomić and S. D. Zarić, *Cryst. Growth Des.*, 2010, **10**, 3901–3908.
18 Z. D. Tomić, D. Sredojević and S. D. Zarić, *Cryst. Growth Des.*, 2006, **6**, 29–31.
19 G. A. Bogdanović, A. Spasojević-de Biré and S. D. Zarić, *Eur. J. Inorg. Chem.*, 2002, 1599–1602.
20 D. Sredojević, G. A. Bogdanović, Z. D. Tomić and S. D. Zarić, *CrystEngComm*, 2007, **9**, 793–798.
21 M. K. Milčić, V. B. Medaković and S. D. Zarić, *Inorg. Chim. Acta*, 2006, **359**, 4427–4430.
22 M. K. Milčic, V. B. Medaković, D. N. Sredojević, N. O. Juranić and S. D. Zarić, *Inorg. Chem.*, 2006, **45**, 4755–4763.
23 S. Roy, M. G. B. Drew, A. Bauzá, A. Frontera and S. Chattopadhyay, *Dalton Trans.*, 2017, **46**, 5384–5397.

24 V. I. Minkin, M. N. Glukhovtsev and B. Y. Simkin, *Aromaticity and Antiaromaticity*, Wiley, New York, 1994.
25 M. K. Milčic, B. D. Ostojić and S. D. Zarić, *Inorg. Chem.*, 2007, **46**, 7109–7114.
26 N. K. Shee and D. Dutta, *Inorg. Chim. Acta*, 2016, **453**, 339–344.
27 E. Kleinpeter and A. Koch, *Phys. Chem. Chem. Phys.*, 2011, **13**, 20593–20601.
28 K. An, T. Shen and J. Zhu, *Organometallics*, 2017, **36**, 3199–3204.
29 S. R. Batten, S. M. Neville and D. R. Turner, *Coordination polymers: design, analysis and application*, Royal Society of Chemistry, Cambridge, 2009.
30 *Design and Construction of Coordination Polymers*, ed. M.-C. Hong and L. Chen, John Wiley & Sons, Inc., Hoboken, New Jersey, 2009.
31 Z.-H. Yan, X.-Y. Li, L.-W. Liu, S.-Q. Yu, X.-P. Wang and D. Sun, *Inorg. Chem.*, 2016, **55**, 1096–1101.
32 D. Sun, L.-L. Han, S. Yuan, Y.-K. Deng, M.-Z. Xu and D.-F. Sun, *Cryst. Growth Des.*, 2013, **13**, 377–385.
33 D. Sun, S. Yuan, H. Wang, H.-F. Lu, S.-Y. Feng and D.-F. Sun, *Chem. Commun.*, 2013, **49**, 6152–6154.
34 Z. Wang, X.-Y. Li, L.-W. Liu, S.-Q. Yu, Z.-Y. Feng, C.-H. Tung and D. Sun, *Chem. – Eur. J.*, 2016, **22**, 6830–6836.
35 W.-M. Chen, X.-L. Meng, G.-L. Zhuang, Z. Wang, M. Kurmoo, Q.-Q. Zhao, X.-P. Wang, B. Shan, C.-H. Tung and D. Sun, *J. Mater. Chem. A*, 2017, **5**, 13079–13085.
36 C. Janiak, *Dalton Trans.*, 2003, 2781–2804.
37 S. Kitagawa, R. Kitaura and S.-I. Noro, *Angew. Chem., Int. Ed.*, 2004, **43**, 2334–2375.
38 M. O'Keeffe and O. M. Yaghi, *Chem. Rev.*, 2012, **112**, 675–702.
39 G. R. Desiraju, J. J. Vittal and A. Ramanan, *Crystal Engineering: A Text Book*, World Scientific, Singapore, 2011.
40 K. Biradha, A. Ramanan and J. J. Vittal, *Cryst. Growth Des.*, 2009, **9**, 2969–2970.
41 M. H. Mir, G. K. Tan, L. L. Koh and J. J. Vittal, *Angew. Chem., Int. Ed.*, 2010, **49**, 390–393.
42 F. Ahmed, S. Roy, K. Naskar, C. Sinha, S. M. Alam, S. Kundu, J. J. Vittal and M. H. Mir, *Cryst. Growth Des.*, 2016, **16**, 5514–5519.
43 B. Dutta, A. Dey, C. Sinha, P. P. Ray and M. H. Mir, *Inorg. Chem.*, 2018, **57**, 8029–8032.
44 B. Dutta, S. M. Pratik, S. Jana, C. Sinha, A. Dutta and M. H. Mir, *ChemistrySelect*, 2018, **3**, 4289–4291.
45 G. M. Sheldrick, *Acta Crystallogr., Sect. A: Found. Crystallogr.*, 2008, **64**, 112–122.
46 J. A. P. M. J. Frisch, G. W. Trucks, H. B. Schlegel, G. E. Scuseria, M. A. Robb, J. R. Cheeseman, J. A. Montgomery, T. Vreven, K. N. Kudin, J. C. Burant, J. M. Millam, S. S. Iyengar, J. Tomasi, V. Barone, B. Mennucci, M. Cossi, G. Scalmani, N. Rega and G. A. Petersso, *Gaussian 03 Package*, 2003.
47 *GAMESS, 2016-Pgi-linux-mkl*, http://www.msg.ameslab.gov/gamess.
48 K. Ruud, T. Helgaker, R. Kobayashi, P. Jørgensen, K. L. Bak and H. J. A. Jensen, *J. Chem. Phys.*, 1994, **100**, 8178–8185.
49 K. Ruud, T. Helgaker, K. L. Bak, P. Jørgensen and J. Oleson, *Chem. Phys.*, 1995, **195**, 157–169.
50 T. Lu and F. Chen, *J. Comput. Chem.*, 2012, **33**, 580–592.
51 V. A. Blatov, *IUCr CompComm Newsletter*, 2006, **7**, 4 http://www.topos.ssu.samara.ru.
52 M. C. Etter, *Acc. Chem. Res.*, 1990, **23**, 120–126.
53 P. v. R. Schleyer, C. Maerker, A. Dransfeld, H. Jiao and N. J. R. v. E. Hommes, *J. Am. Chem. Soc.*, 1996, **118**, 6317–6318.
54 P. R. v. Schleyer and H. Jiao, *Pure Appl. Chem.*, 1996, **68**, 209–218.
55 A. Stanger, *J. Org. Chem.*, 2006, **71**, 883–893.
56 E. Maslowsky, *Coord. Chem. Rev.*, 2011, **255**, 2746–2763.
57 J. O. C. Jiménez-Halla, E. Matito, J. Robles and M. Solà, *J. Organomet. Chem.*, 2006, **691**, 4359–4366.
58 Z. Chen, C. S. Wannere, C. Corminboeuf, R. Puchta and P. V. R. Schelyer, *Chem. Rev.*, 2005, **105**, 3842–3888.
59 S. G. Patra and D. Dutta, *Comput. Theor. Chem.*, 2017, **117**, 55–60.
60 Z. Chen, C. S. Wannere, R. Puchta and P. V. Rague, *Chem. Rev.*, 2005, **105**, 3842–3888.
61 J. J. Torres-Vega, A. Vásquez-Espinal, J. Caballero, M. L. Valenzuela, L. Alvarez-Thon, E. Osorio and W. Tiznado, *Inorg. Chem.*, 2014, **53**, 3579–3585.
62 R. Báez-Grez, W. A. Rabanal-León, L. Alvarez-Thon, L. Ruiz, W. Tiznado and R. Pino-Rios, *J. Phys. Org. Chem.*, 2018, e3823.
63 N. Menges and I. Bİldİrİcİ, *J. Chem. Sci.*, 2017, **129**, 741–752.
64 R. Báez-Grez, L. Ruiz, R. Pino-Rios and W. Tiznado, *RSC Adv.*, 2018, **8**, 13446–13453.
65 A. D. Becke and K. E. Edgecombe, *J. Chem. Phys.*, 1990, **92**, 5397–5403.
66 J. C. Santos, W. Tiznado, R. Contreras and P. Fuentealba, *J. Chem. Phys.*, 2004, **120**, 1670–1673.
67 J. C. Santos and P. Fuentealba, *Chem. Phys. Lett.*, 2007, **443**, 439–442.
68 F. Fuster, A. Savin and B. Silvi, *J. Phys. Chem. A*, 2000, **104**, 852–858.
69 J. C. Santos, J. Andres, A. Aizman and P. Fuentealba, *J. Chem. Theory Comput.*, 2005, **1**, 83–86.
70 D. L. Wood and J. Tauc, *Phys. Rev. B: Condens. Matter Mater. Phys.*, 1972, **5**, 3144–3151.
71 S. Halder, A. Dey, J. Ortega-Castro, A. Frontera, P. P. Ray and P. Roy, *J. Phys. Chem. C*, 2016, **120**, 25557–25563.
72 J. N. Wei, Y. L. Zhang, Y. Chi, L. Liu, W. X. Zhang and Z. F. Xi, *J. Am. Chem. Soc.*, 2016, **138**, 60–63.
73 R. Grande-Aztatzi, J. M. Mercero, E. Matito, G. Frenking and J. M. Ugalde, *Phys. Chem. Chem. Phys.*, 2017, **19**, 9669–9675.
74 M. Dimitrova and D. Sundholm, *Phys. Chem. Chem. Phys.*, 2018, **20**, 1337.

